The Astrophysical Journal, 838:138 (7pp), 2017 April 1 https://doi.org/10.3847/1538-4357/aa656c

Are All Flare Ribbons Simply Connected to the Corona?*

Philip G. Judge[1], Alin Paraschiv[2,3], Daniela Lacatus[2,3], Alina Donea[2], and Charlie Lindsey[4]
[1] High Altitude Observatory, National Center for Atmospheric Research, P.O. Box 3000, Boulder, CO 80307-3000, USA; judge@ucar.edu
[2] Monash Center for Astrophysics, School of Mathematical Science, Monash University, Victoria 3800, Australia; alina.donea@monash.edu
[3] Institute of Geodynamics "Sabba S. Stefanescu" of the Romanian Academy, 19-21, str. J. L. Calderon, Bucharest, Romania
alin.paraschiv@monash.edu, daniela.lacatus@monash.edu
[4] Northwest Research Associates, 3380 Mitchell Lane, Boulder, CO 80301, USA; indsey@cora.nwra.com
Received 2016 September 13; revised 2017 March 1; accepted 2017 March 2; published 2017 April 3

Abstract

We consider the observational basis for the belief that flare ribbons in the chromosphere result from energy transport from the overlying corona. We study ribbons of small flares using magnetic and intensity data from the *Hinode*, *Solar Dynamics Observatory*, and *IRIS* missions. While most ribbons appear connected to the corona and overlie regions of significant vertical magnetic field, we examine one ribbon with no clear evidence for such connections. Evolving horizontal magnetic fields seen with *Hinode* suggest that reconnection with preexisting fields below the corona can explain the data. The identification of just one, albeit small, ribbon, with no apparent connection to the corona, leads us to conclude that at least two mechanisms are responsible for the heating that leads to flare ribbon emission.

Key words: Sun: chromosphere – Sun: flares – Sun: magnetic fields – Sun: UV radiation – techniques: polarimetric

Supporting material: animation

1. Introduction

The purpose of the present paper is to test the hypothesis that flare ribbons are always associated with the downward transport of energy released in the corona. These ribbons are locations where much of the flare energy is radiated back into space. Specifically, we will analyze a ribbon reported as being caused by "nanoflaring" activity, motivated by the peculiar environment in which this ribbon seems to exist, and noting that the presence of ribbons is characteristic of flares of all sizes. Figure 1 shows the environment prior to the brightening of the ribbon under study, as well as the ribbon itself some minutes later, as seen in the 304 Å channel using data from the AIA instrument (Lemen et al. 2012) on the *Solar Dynamics Observatory* (*SDO*).

Ribbons are taken to be one signature of a universal process involving magnetic reconnection. In this "standard model" of flares (Carmichael 1964; Sturrock 1966; Hirayama 1974; Kopp & Pneuman 1976), nonthermal energy assumed to be stored for some time in the corona is suddenly released (Gold & Hoyle 1960). The energy propagates away from the release site in the corona. When propagating downward, bright ribbons and kernels of radiation are observed as this directed energy is dissipated in dense chromospheric plasma.

The basic hypothesis of the standard model is supported by a considerable wealth of evidence (see Fletcher et al. 2011, for a recent review). The advent of routine hard X-ray (HXR) data simultaneously with soft X-rays and EUV/UV data from modern spacecraft has confirmed that HXR emission arises from bremsstrahlung radiation emitted as energetic electrons impact the denser chromosphere (Brown 1971). The connection between energetic electron precipitation and flare ribbons has become generally accepted.

A particularly clear example of the magnetic corona–chromosphere connection is seen in Figure 3 of Sadykov et al. (2016). Yet there are indications that the relationship between energy propagating down from the corona and that observed coming from the denser layers is not quite this straightforward. For example, flare ribbons are bright in regions where HXRs are undetectable as well as bright (e.g., Section 3.3 of Fletcher et al. 2011). A clear example of a bright ribbon covering a more extended area than HXR emission is shown in Figure 1 of Judge et al. (2015). Quoting from Fletcher et al. (2011), "In general the HXR sources are confined to localized areas situated on the outer edges of the elongated flare ribbons observed in UV and Hα and are predominantly associated with bright Hα/UV kernels…" What, then, is the relationship between beams of particles and, more generally, energy transport, from the corona to the flare ribbons? The question is of some importance, for if energy is stored and released in regions other than the corona, then the mechanism for flare energy storage and release is not restricted to the corona, i.e., the standard model does not describe all flares.

Recently Testa et al. (2014, hereafter T2014) used *IRIS* data (De Pontieu et al. 2014) to infer the presence of nonthermal particles by combining data from *IRIS* with synthetic data. The synthetic data are required because an instrument like *IRIS* cannot by itself be used to infer nonthermal particles. T2014 conclude, "The observable that discriminates most efficiently between the beam heating models and the conduction models is the Doppler shift in the Si IV emission." We note that the post-impulsive dynamics as reflected in Si IV or other UV emission is far removed from the energy transport and dissipation mechanisms. Thus, we ask whether other scenarios for energy storage and release might be acceptable.

We decided to reexamine the data examined by T2014. For most of their ribbons, magnetic data (and "moss" emission) support the idea that a coronal magnetic connection exists prior to the ribbon emission (see the ellipses in Figure 1). However, the ribbon highlighted by white lines in this figure has no clear connections to the overlying corona, and that appears to be

* The National Center for Atmospheric Research is sponsored by the National Science Foundation.

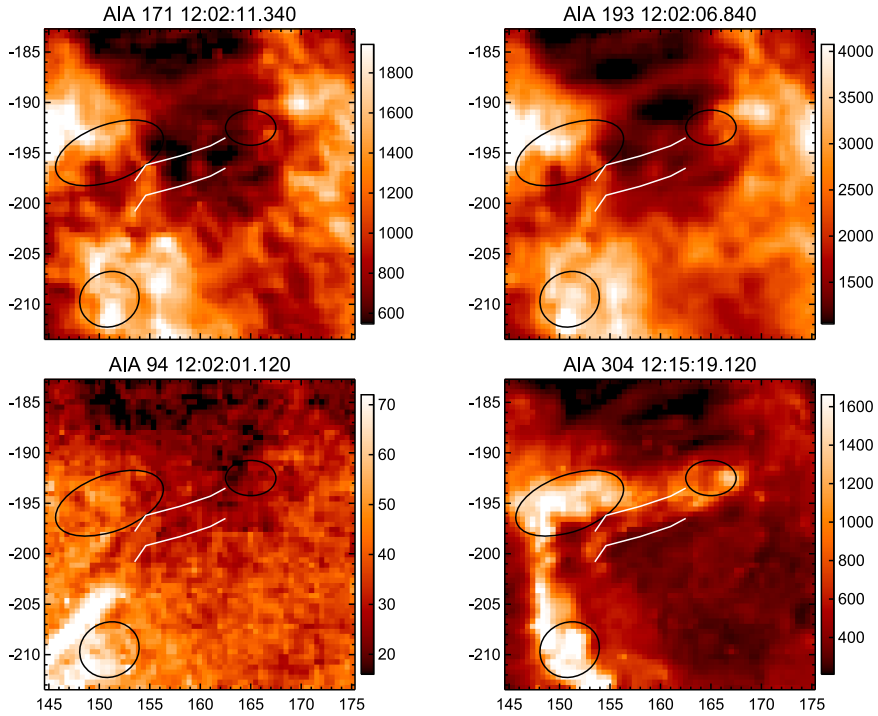

Figure 1. Intensity data from the AIA instrument on the *SDO* spacecraft are shown as a function of heliographic solar X and solar Y coordinates, in arcseconds. The field of view spans part of AR 11890 on 2013 November 9. The data reflect the chromospheric and coronal environment surrounding the flare ribbon under examination. In AIA data, the ribbon is seen most clearly, at 12:15:19 UT, in the 304 Å band (predominantly He II) in the bottom right panel. All other panels show conditions prior to the ribbon's appearance, close to 12:02 UT. The ribbon lies between the two white lines. Black ellipses identify regions where, during the brightening at 12:15:19 UT, the 304 Å emission is associated with moss emission and vertical magnetic field (see Figure 3). Typical moss emission is seen all around the ribbon in the bright patches of network plage emission, for example, at $X = 170$, $Y = -190$. The color bars label instrument DN values.

incompatible with the standard model. This particular ribbon drew our attention when comparing the image of 1400 Å with that of 193 Å in Figure 1 of T2014, taken during the outburst. We noticed the dramatic differences in the relative brightness of the ribbon (1400/193 Å brightnesses) compared with the surrounding network footpoints. The latter are identified as those regions where the accompanying "hot" 94 Å loops end. We noted that the ribbon of interest (ROI) is far more intense relative to the coronal emission during the flare. Our Figure 1 shows data acquired before the flare, also showing that the overlying "moss" emission (patchy emission at 171 and 193 Å) has a different morphology, with essentially zero emission seen across half of the area later covered by the ribbon.

It is these differences that lead us to ask whether all flare ribbons result from energy transport down from the corona. For without our careful observations, one is led to conclude that the ROI is merely yet another manifestation of the processes captured by the standard model. T2014 modeled part of this ribbon *assuming* the standard model. Indeed, both power-law distributions and arguments concerning the universal nature of reconnection in space physics support the notion that flare physics might be independent of scale (e.g., Nishizuka et al. 2009; Shibata & Takasao 2016; Sharma et al. 2016). Our work should be viewed as a test of the general validity of the standard model as applied to solar flare ribbon phenomena.

2. Observational Analysis

2.1. UV and EUV Data

We refer to T2014 for the circumstances of the *IRIS* and other observations of active region (AR) 11890 on 2013 November 9. Figure 2 shows images of interest from *IRIS* and the AIA instrument. The ribbon of central interest here contains the point "D" analyzed by T2014, lying 252″ SW of Sun center. The local vertical is $\vartheta = 15°$ from the line of sight, with $\mu = \cos\vartheta = 0.96$. We will refer to this ribbon as the "ROI."

During the *IRIS* observations, the chromospheric ribbon brightened twice, of which only the first, weaker event was discussed by T2014. Here we concentrate on the second brightening, which is similar in morphology. This makes no difference to our conclusions because we examine the magnetic connectivity between the corona and ribbon prior to both brightenings. The bright ribbon is clearly seen at its brightest phase (12:15:41 UT) in the lower left panel of Figure 2. This ribbon's locus is traced in the other images using white lines.

The ribbon is barely seen in the 1600 Å AIA channel, which admits contributions from the UV continuum, the resonance lines of C IV, and the Balmer-α line of He II (1640 Å). It is clearly seen in the Mg II slit-jaw image (Figure 2), which forms across the entire chromosphere. The AIA image at 94 Å appears superficially to overlap with the ribbon. However, in movies S1 and S2 published by T2014, the 94 Å emission clearly originates from closer to the larger UV flaring patch seen near $(X, Y) = (167, -192)$, highlighted with a black ellipse in our figures. The 94 Å coronal emission appears close to but over the ROI in a loop-like structure connected to the region of the 150 G line-of-sight field, near (167, −192). We have examined all other channels from the AIA instrument between 12:15 and 12:16 UT. The clearest indicator of the ROI seen in AIA data is in the 304 Å channel (mostly He II). It is not detected in the 1700 Å UV continuum channel, but during the

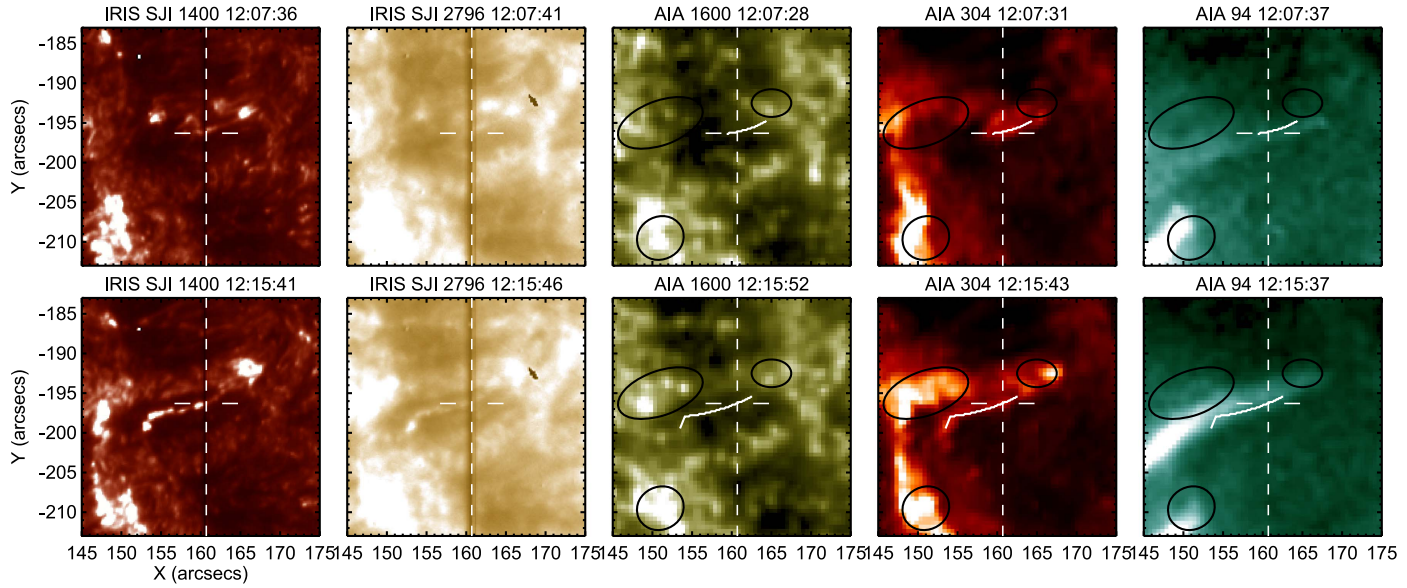

Figure 2. Intensity data are shown for AR 11890 on 2013 November 9, corresponding to two small flaring events associated with the ROI. Upper panels show the weaker 12:07 flare ribbon analyzed by Testa et al. (2014). Lower panels show the stronger flaring peaking at 12:15. All panels have been co-aligned by eye to approximately 0.″3. The solar coordinates are referred to the coordinate system specified in the headers. Only a $30'' \times 35''$ field of view is shown, to highlight the precise position of the flare ribbon traced in all panels except for the slit-jaw *IRIS* panels. As before, point "D" of Figure 2 in T2014 is marked by the intersection of the vertical dashed line with the short horizontal marked line.

ribbon's brightening there are hints of weak emission at 171, 193, 211, and 335 Å, all coronal bands.

In conclusion, the near absence of 1600 Å ribbon emission and its presence in lines from Mg II to He II indicate that the ROI's emission originates from the mid- to upper chromosphere and the transition region.

2.2. Magnetic Data

Figure 3 shows magnetic parameters inverted from raster scans with the SP instrument on the *Hinode* spacecraft (Lites et al. 2008). We used data from the CSAC at HAO based on the code MERLIN. The coordinates are all rotated to a reference frame close in time to the two ribbon flaring events obtained using the HMI instrument (Schou et al. 2012) on *SDO*. Given the small size of the ribbons, however, we chose to base our further analysis on the *Hinode* raster scans, due to the higher spatial resolution and magnetic sensitivity. In spite of the evolution of solar features during the *Hinode* scans (the 30″ widths of the images shown took ≈6 minutes, comparable to a granule lifetime), the *Hinode* images shown have been successfully co-aligned to those of HMI to $\approx \pm 0.''3$. The magnetic data are striking. There is essentially just noise in the line-of-sight (longitudinal) component of the field B_L near the ROI. The *Hinode* data give a mean value of 11 ± 10 G for the longitudinal field calculated from areas extending 2″ around the ribbon loci shown. The noise in longitudinal field acquired with the SP corresponds to just 3 Mx cm^{-2} in each spatial pixel (Lites et al. 2008). The average *Hinode* tangential (near-horizontal) field component B_T is 73 ± 24 G.

If similar connections existed from the ROI, it would have several such origins distributed along its locus in the 94 Å or other coronal images.

The raster scans from the *Hinode* spectropolarimeter shown in Figure 3 were obtained about 1 hr before and 6 hr after the flaring activity. An intermediate scan was started but failed during the flaring period; it contains no useful data. But from the data shown, three characteristics caught our attention. First, the 200 G horizontal flux seen near the ROI before the flaring is replaced by 200 G vertical field components hours after the flare. Second, the azimuth of the field in the neighborhood of the ROI before the flare has significant spatial coherence, with a mean value close to $44^{\circ}{}^{+31}_{-27}$ relative to the N–S direction. This aspect suggests, albeit weakly, the presence of an emerging magnetic field roughly along the same direction as the long axis of the ribbon. An HMI time-series animation of the field evolution in between the two *Hinode* raster scans is provided in the online animated version of Figure 3. HMI unfortunately does not have the sensitivity to reveal horizontal fields in the upper photosphere of the ROI during this period.

3. Discussion

T2014 recognized that chromospheric reconnection might explain some of their data: "Chromospheric reconnection could in principle provide an alternative explanation for the observed chromospheric and TR variability.... The moss brightenings *clearly occur at conjugate footpoints of hot loops undergoing heating, and there is a clear correlation between the coronal and chromospheric/TR emission*, naturally explained by beam heating."

Above, we have added italics to those statements that appear to be inconsistent with the ROI. It is important to note that all other bright ribbons and kernels lie above or close to regions with detectable longitudinal fields. The absence of a longitudinal field above about 10 G in the photosphere near the ROI suggests that there is little magnetic flux emerging through this region into the corona.

3.1. The Magnetic Field prior to the Flaring of the ROI

The question of connection of the ribbon to the overlying corona concerns only the connection between chromosphere and corona (such small flares generate undetectable changes in deeper layers). The magnetic field threading the chromosphere

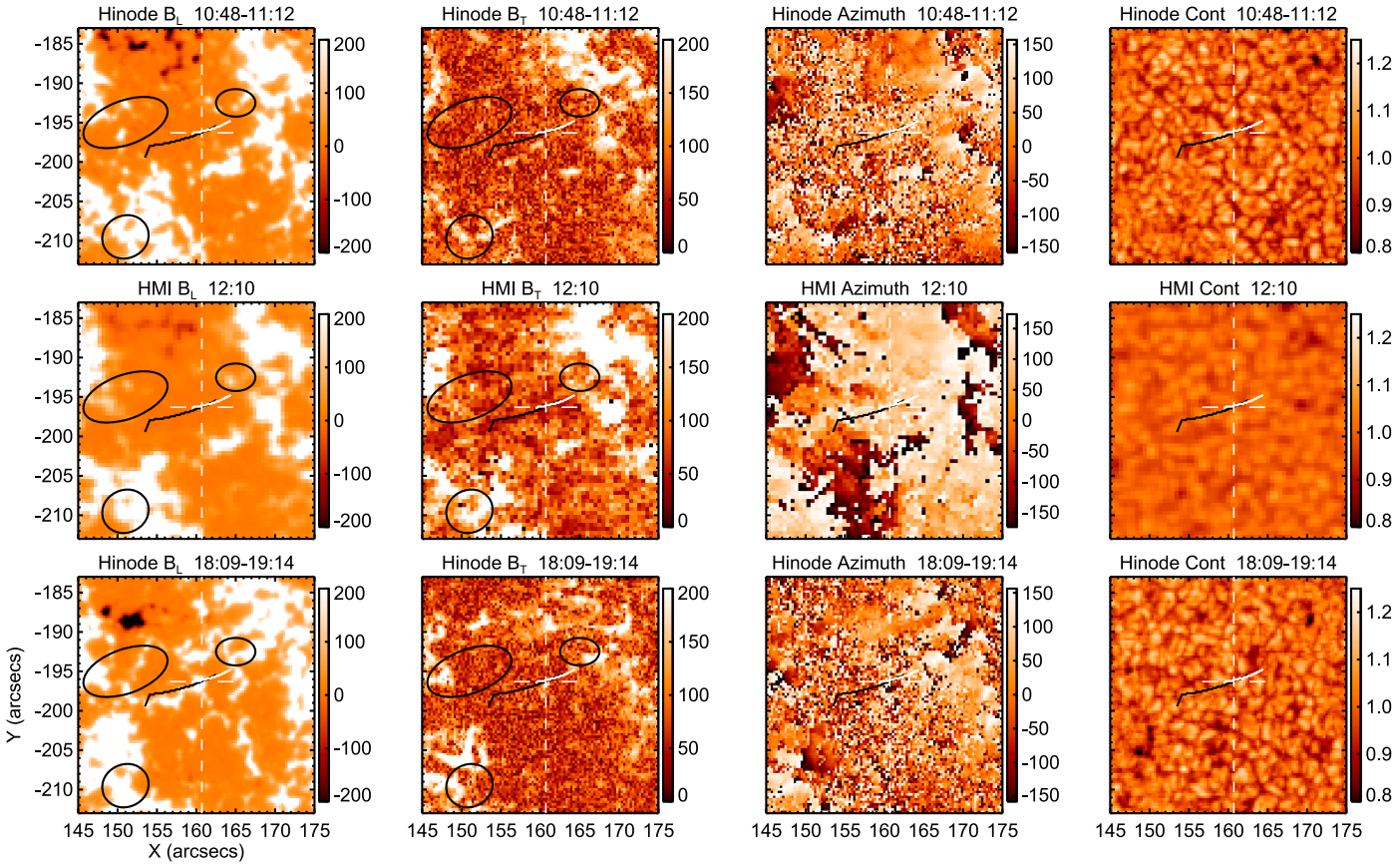

Figure 3. Magnetic data are shown for AR 11890, before, during, and after the two flares at 12:07 (ribbon extent traced with a white line) and 12:15 (black line) shown in Figure 2. Each row shows longitudinal, tangential fields, field azimuth (with the 180° ambiguity unresolved), and the continuum intensity. The upper panels show the *Hinode* scan obtained before the flares, the middle panels show HMI data closest to the flaring events, and the lower panels show *Hinode* data from the next complete scan some 6 hr later. Six hours is a considerable fraction of the lifetimes of supergranules, so surface field evolution has occurred between the two *HINODE* scans. High-cadence HMI magnetic field evolution animation for the time range in between the two *Hinode* scans is available in the online version of this figure.

(An animation of this figure is available.)

must span several scale heights and must therefore be significantly different than measured in the photosphere, which therefore presents a difficulty. But given the measured photospheric fields, it is hard to see from where a chromospheric field connected upward might originate. The entire stratified chromosphere spans about 1500 km, which corresponds to $\approx 2''$. In Figure 3 the ribbon is encased in a void of field with values $\lesssim$10 G extending at least $2''$ all around the ribbon. We already noted the absence of moss emission in this area (Figure 1 of T2014).

Some weak longitudinal field may suffice to provide unseen connections to the corona along the ribbon. Indeed, a field is present to the south of both ends of the ROI, of the same polarity, 30–40 G in strength and covering just a couple of square arcseconds (see the *Hinode* panel B_L in the top left of Figure 3). These fields are not visible in HMI by the time of the flare, 1^h22^m later (second row of the figure). These small concentrations are some $5''$ from the center of the ROI. Could longitudinal fields such as these have been advected to the locus of the ROI by known surface motions in time for a coronal connection to be established? Berger et al. (1998) studied surface diffusion rates around ARs, finding a coefficient of $\kappa \approx 80\,\mathrm{km^2\,s^{-1}}$ for several tens of minutes. In the $t = 100$ minutes after the first *Hinode* scan, elements would diffuse a distance of $\frac{1}{3}\sqrt{\kappa t} = \frac{1}{3}\sqrt{80 \times 6000} \approx 200$ km, which is an angular distance of $0\farcs3$. Supergranular diffusion in regions far from strong fields is larger, with $\kappa \lesssim 800\,\mathrm{km^2\,s^{-1}}$. Even with such a high rate of diffusion, the surface diffusion would have to accumulate from within a distance of $1''$ of the ribbon and produce vertical components along the ROI in the beam-heating scenario. This seems unlikely given the quasi-random nature of this diffusion implicit in the work of Berger et al. (1998).

3.2. The Magnetic Field after the Disappearance of the ROI

In the 6 hr between the flare and the second *Hinode* scan, relatively strong post-flare longitudinal "network" fields appear in the lowest panel of Figure 3. It is seen meandering underneath the position of the ROI, with a length $\ell \approx 10''$. Emergence and/or surface diffusion of field must be responsible for this new network flux. The new network flux amounts to $\Phi \approx 200$ G times the apparent area of the network, $\approx 1'' \times \ell'' \equiv 5 \times 10^{16}\,\mathrm{cm^2}$, so that $\Phi \approx 10^{19}$ Mx. To build this flux from the mean pre-ribbon longitudinal field strength of 10 G, this flux would have to have collected, merged, and strengthened from an area of about 200 square arcseconds, about 100 $\mathrm{Mm^2}$. This area is far larger than the area available for diffusion in the time available, which we write as $L\ell \approx \frac{1}{3}\kappa\, 21600 \approx 6\,\mathrm{Mm^2}$, even using $\kappa \approx 800\,\mathrm{km^2\,s^{-1}}$.

It seems that some flux emergence into the chromosphere occurred between the first and second *Hinode* scans. Such flux

emergence is below the detection limit for HMI (row 2, column 2 of Figure 3) but is hinted at by the coherent horizontal field seen in the first *Hinode* scan (row 1, column 2 of Figure 3). We suggest that this flux emergence might help explain the presence of the ROI, in particular, the horizontal fields that appear somewhat close to the ribbon in the pre-ribbon *Hinode* scan strongly indicate horizontal flux. The series of HMI vector field maps was examined between 09:58 and 20:10 UT; from 11 to 19 UT is shown in the online animated version of Figure 3. From this movie, any horizontal fields are too noisy to be seen as any coherent structure rising through the photosphere. Beginning close to 18:00 UT, the longitudinal field patch close to (−165, −201) migrated quickly toward the position of the clump of flux seen underlying the ROI in the last *Hinode* (18:09–19:14 UT) scan.

Even if we cannot conclusively detect horizontal emerging flux, we can conclude that the magnetic conditions around the ROI are qualitatively different from the other ribbons discussed by T2014.

3.3. Energy Requirements and the Coronal Magnetic Field

But can we discount a coronal origin for the ROI? Let us consider the energy requirements; for this we can use Figure 3 of T2014. From this figure we see that the Mg II k line has excess emission averaging 400 DN/s/spatial pixel for a period of 200 s. Using calibration factors from *SolarSoft* routine `iris_get_response.pro`, we find that the intensity of Mg II k is $I_k = 1.5 \times 10^5$ erg cm^{-2} s^{-1} sr^{-1}. The k line contributes ≈10% of the total chromospheric radiative losses known in 1981 (Table 29 of Vernazza et al. 1981), and allowing for a doubling of the losses due to the inclusion of Fe II lines (Anderson & Athay 1989b), we find that the excess emission is $\approx 20 \times 4\pi I_k \approx 4 \times 10^7$ erg cm^{-2} s^{-1}. The same calculation for the Si IV λ1403 line gives an excess intensity of 6×10^3 erg cm^{-2} s^{-1} sr^{-1}, 25 times smaller than seen in the k line.

We assume that we have a field strength of 10 G, corresponding to the 3σ upper limit, emerging from the region of the ROI into the corona. (Below we relax this assumption.) The total energy per unit area in a straight tube of length L is $LB^2/8\pi$, which for $L \approx 10^{10}$ cm (100 Mm, as used by T2014) and $B \lesssim 10$ G gives $\lesssim 4 \times 10^{10}$ erg cm^{-2}. The 304 Å frame in movie "S2" of T2014 shows that the heating of the ROI continues beyond the time span of the *IRIS* sequence, which ends at 12:17:16 UT. Thus, we can set a time $\gtrsim 10^2$ s for the duration of the heating. Therefore, the overlying corona can supply $\lesssim 4 \times 10^8$ erg cm^{-2} s^{-1} of magnetic power per unit area into the chromosphere below. If, optimistically, we assume that 10% of the magnetic energy along this tube is free energy available, then just $\lesssim 4 \times 10^7$ erg cm^{-2} s^{-1} is available. This is close to the energy requirements of the quiet-Sun chromosphere (Anderson & Athay 1989a) and our excess estimate above. An alternative limit can be derived using the Alfvén crossing time for the tube, which is L/V_A. With a pre-flare coronal gas pressure $p \approx 0.1$ dynes cm^{-2} (Jordan 1992), $T = 10^6$ K, we have a density $\rho \approx 2 \times 10^{-15}$ g cm^{-3} and $V_A \lesssim 700$ km s^{-1}. Then $L/V_A \gtrsim 140$ s.

The energy available in a coronal tube is formally enough to account for the radiation losses from the chromosphere below. But our estimate is a strict upper limit for the following reasons: (1) We have used the 3σ "detection" of longitudinal field from the *Hinode* scan 1 hr before the flare, and the energy is $\propto B_L^2$. The field strength in the overlying corona is surely lower than the 10 G upper limit in the photosphere. (2) The energy is $\propto L$, and L has been taken from neighboring coronal structures seen clearly in the 94 Å channel that are rooted in far stronger concentrations. (3) We have assumed that 10% of *all* the magnetic energy is available for release within the tube. (4) We have assumed that sufficient time exists for this energy to be released. Reconnection typically takes place at $0.1V_A$, through complex dynamical mechanisms such as the plasmoid instability (e.g., Bhattacharjee et al. 2009). Thus, the dynamical time for energy release becomes too long, $L/0.1V_A \approx 1400$ s.

It appears that the ROI cannot be reconciled by heating from the overlying corona. Either the dynamical time is too long ($L = 100$ Mm) or, if L is small enough to account for the dynamical time, the free energy $\propto L$ is insufficient to account for the observed losses.

Now let us permit the coronal connection to include the *transverse* component of the field, as well as the longitudinal component. Then we expect the connection to the corona to be highly oblique to the line of sight, as is seen in the 94 Å image (Figure 2). In this case the energy available is some 50 times bigger and the Alfvén speeds seven times larger. In this case, the observations are reconciled with a beam-heating picture: the energy release rate from the corona is $\lesssim 2 \times 10^9$ erg cm^{-2} s^{-1} and the dynamical time is about 200 s, compared with about 2×10^7 erg cm^{-2} s^{-1} and 100 s, respectively.

But is this scenario credible? The morphology of the horizontal field and the absence of moss coronal emission simply do not support the idea that the fields detected are connected to the corona.

3.4. Local Heating

We are forced to consider *local* sources of heating for the ROI. The tangential field in the *Hinode* scan is around 75 G. Let us consider the emergence of a near-horizontal tube of flux through the chromosphere in a quasi-steady state prior to some energy release process. It emerges into a preexisting field in the upper chromosphere in the AR where a preexisting canopy field exists, fields rooted elsewhere in stronger concentrations that have turned horizontal to ensure pressure balance as the chromospheric gas pressure drops well below the magnetic pressure. The total energy density available in an emerging tube with this field strength is $B_T^2/8\pi \approx 220$ erg cm^{-3}. The Alfvén speed is roughly $B_T/\sqrt{4\pi\rho_u} \approx 200$ km s^{-1}, where $\rho_u \approx 10^{-12}$ g cm^{-3} is the density in the upper chromosphere. Let us assume that the tube emerges into canopy fields, rooted in more distant network patches, of a lower strength. To estimate this strength, we note that in the neighborhood of the ribbon the longitudinal flux is all of the same sign, and the average longitudinal flux density over a region centered at the ribbon is about 55–80 Mx cm^{-2}, depending on the local area chosen. For the surrounding $20'' \times 20''$ area (of order one supergranule in size) the average is 80 Mx cm^{-2}. We envisage that the locally emerging flux begins to reconnect with the canopy field and generate the extra emission in the ROI. To account for the ribbon, we require, as above, 4×10^7 erg cm^{-2} s^{-1} for about 200 s. Once the reconnection starts, it will proceed at a rate close to $0.1V_A'$, where V_A' is the Alfvén speed in the reconnecting component of the field. If the angle between the emerging tube and the canopy fields is ϑ, then $V_A' = V_A \sin\vartheta$ Thus, the reconnection will convert

magnetic into thermal energy at the rate

$$\mathcal{F} \lesssim 0.1 \sin^3\vartheta \frac{B_T}{\sqrt{4\pi\rho_u}} \frac{B_T^2}{8\pi} \lesssim 5 \times 10^7 \text{ erg cm}^{-2}\text{ s}^{-1}, \quad (1)$$

where we have used $\sin\vartheta = 0.5$ as a rough estimate of the mismatch in directions of the horizontal and canopy fields. It seems that there is power available from chromospheric reconnection to drive the radiation losses seen in the ROI. With a (vertical) inflow speed into the reconnection layer of $0.1 \sin\vartheta V_A \approx 25$ km s^{-1}, lasting for ≈200 s, the reconnection advects a total mass per unit area of $m_R = 2.5 \times 10^6 \times 200\rho_u = 5 \times 10^{-4}$ g cm^{-2} from the chromosphere into the reconnection layer. If this partially ionized plasma is heated via dynamical instabilities (e.g., the plasmoid instability; Bhattacharjee et al. 2009) or kinetic processes (ion–neutral collisions, for instance), then this emerging flux effectively leads to heating in the upper chromosphere for column masses above $m_R = 5 \times 10^{-4}$ g cm^{-2}. Interestingly, this corresponds roughly to the range of heights between which the proposed beam dissipation arises in the models of T2014 (Figure S4). Therefore, we would expect similar dynamical signatures from this type of heating to those from beam heating when the reconnected field has access to the overlying corona.

3.5. Can We Refute Chromospheric Reconnection for the ROI?

One might argue that the chromosphere remains "closed" rather than open to the overlying corona, and therefore that lines formed are trapped in closed field lines under a low-β regime in which significant line shifts observed in Si IV cannot be observed. However, in this picture we envisage plasma mass advected into the canopy fields, which are themselves open to the overlying corona, a process commonly called "interchange reconnection." We would naturally expect the *same* kind of dynamics along one of the canopy field lines as computed in the beam heating scenario, since both result from deposition of energy in plasma of similar column masses, which later enters via reconnection a tube of field that is connected to the corona. This ambiguity reminds us of the sobering reality that lines such as Si IV are like a dog with two masters—both the corona and chromosphere have significant effects on such transition-region lines. Also, it must be remembered that Si IV intensities are a factor of 25 weaker than the Mg II lines. Thus, these lines reflect only a small fraction of the energy release and its properties in the evolving atmosphere.

A common reason for discounting chromospheric reconnection is that the ribbons "light up" between observations separated by tens of seconds, and that there is nothing that can physically communicate one part of the chromosphere to reconnect on these timescales. But this is not correct near ARs with transverse fields of order 70 G. The ROI has a horizontal extent of about 7 Mm (Figure 2), so it would take just 14 s for magnetic perturbations, such as a tearing mode, to propagate horizontally across the surface. Further, an emerging flux rope defines a ribbon-line morphology as it interacts with the overlying fields. Therefore, we respectfully disagree with the dismissal of chromospheric reconnection discussed in Section S3 of T2014, in the case of the ROI.

Finally, a widely held belief that the chromosphere is highly dynamic has arisen from studies seeking dynamical phenomena associated with the chromosphere (e.g., de Pontieu et al. 2007). The question would then arise whether the upper chromosphere would shred a rope of horizontal flux before it could interact with preexisting fibrils extending across supergranular cells. But this is a nonissue since simple estimates of such things as spicules and related phenomena show them to cover no more than 0.1% of the solar surface area and to originate at supergranular vertices. Spectral observations of the solar disk with HRTS by Dere et al. (1983) show that both line widths and shifts very rarely approach those of the dynamic type II spicules reported by de Pontieu and colleagues. It is also clear from narrowband imaging observations of spectral lines formed in the upper chromosphere, such as the Ca II infrared triplet lines, that fibril structures are stable on timescales of hours or more (e.g., Cauzzi et al. 2008).

4. Conclusions

We have shown that at least one of the several low-energy flare ribbons analyzed by T2014 is very probably magnetically disconnected from the corona. Sufficient energy exists in the emerging magnetic field for local dissipation in the upper chromosphere to account for the observed behavior. Our analysis therefore refutes the statement (T2014) for at least one flare ribbon: "Our analysis provides tight constraints on the properties of such electron beams and new diagnostics for their presence in the non-flaring corona." Care is needed in the interpretation of data from UV instruments like *IRIS*, where the UV spectra are the end step of a series of complex nonlinear phenomena, including the elusive heating terms in the energy equation, otherwise known as the long-standing "coronal heating problem."

In conclusion, there are at least two processes that can lead to the enhanced radiation seen in small flare ribbons, one of which does *not* rely on energy transport from the overlying corona.

Lastly, we note that the ribbons are small events compared with large flares. It remains to be seen whether bigger events can be found in which an energetic connection to the corona can be refuted.

Hinode SOT/SP inversions were conducted at NCAR under the framework of the Community Spectro-polarimetric Analysis Center (CSAC; http://www.csac.hao.ucar.edu/). This work was carried out during a visit to Monash University by P.G.J. and visits of D.L., A.P., and A.D. to HAO, supported by HAO visitor funds and the School of Mathematical Science, Moansh University. We are grateful to a patient referee, in particular for their help in clarifying the observational motivation behind this work.

References

Anderson, L., & Athay, R. 1989a, ApJ, 346, 1010
Anderson, L. S., & Athay, R. G. 1989b, ApJ, 336, 1089
Berger, T. E., Löfdahl, M. G., Shine, R. A., & Title, A. M. 1998, ApJ, 506, 439
Bhattacharjee, A., Huang, Y.-M., Yang, H., & Rogers, B. 2009, PhPl, 16, 112102
Brown, J. C. 1971, SoPh, 18, 489
Carmichael, H. 1964, NASSP, 50, 451
Cauzzi, G., Reardon, K. P., Uitenbroek, H., et al. 2008, A&A, 480, 515
de Pontieu, B., McIntosh, S., Hansteen, V. H., et al. 2007, PASJ, 59, 655
De Pontieu, B., Title, A. M., Lemen, J. R., et al. 2014, SoPh, 289, 2733
Dere, K. P., Bartoe, J.-D. F., & Brueckner, G. E. 1983, ApJ, 267, L65
Fletcher, L., Dennis, B. R., Hudson, H. S., et al. 2011, SSRv, 159, 19
Gold, T., & Hoyle, F. 1960, MNRAS, 120, 89
Hirayama, T. 1974, SoPh, 34, 323
Jordan, C. 1992, MmSAI, 63, 605

Judge, P. G., Kleint, L., & Sainz Dalda, A. 2015, ApJ, 814, 100
Kopp, R., & Pneuman, G. 1976, SoPh, 50, 85
Lemen, J. R., Title, A. M., Akin, D. J., et al. 2012, SoPh, 275, 17
Lites, B. W., Kubo, M., Socas-Navarro, H., et al. 2008, ApJ, 672, 1237
Nishizuka, N., Asai, A., Takasaki, H., Kurokawa, H., & Shibata, K. 2009, ApJL, 694, L74
Sadykov, V. M., Kosovichev, A. G., Sharykin, I. N., Zimovets, I. V., & Vargas Dominguez, S. 2016, ApJ, 828, 4
Schou, J., Scherrer, P. H., Bush, R. I., et al. 2012, SoPh, 275, 229
Sharma, A. S., Aschwanden, M. J., Crosby, N. B., et al. 2016, SSRv, 198, 167
Shibata, K., & Takasao, S. 2016, in Magnetic Reconnection, ed. W. Gonzalez & E. Parker (Basel: Springer), 373
Sturrock, P. A. 1966, Natur, 211, 695
Testa, P., De Pontieu, B., Allred, J., et al. 2014, Sci, 346, 1255724
Vernazza, J., Avrett, E., & Loeser, R. 1981, ApJS, 45, 635